J Eng Math (2009) 63:121–133
DOI 10.1007/s10665-008-9246-y

Numerical approximation of bioluminescence tomography based on a new formulation

Xiaoliang Cheng · Rongfang Gong · Weimin Han

Received: 23 November 2007 / Accepted: 26 August 2008 / Published online: 19 September 2008

Abstract Bioluminescence tomography (BLT) is a promising new method in biomedical imaging. The BLT problem is an ill-posed inverse source problem, usually studied through a regularization technique. A new approach is proposed for solving the BLT problem based on an adjoint equation. Numerical examples show that the new formulation allows us to obtain accurate solutions.

Keywords Bioluminescence tomography · Finite-element methods · Inverse problem

1 Introduction

Molecular imaging is a rapidly developing biomedical imaging technique for studying physiological and pathological processes *in vivo* at the cellular and molecular levels; see e.g. [1–5] and references therein. The goal of molecular imaging is to depict non-invasively cellular and molecular processes *in vivo* sensitively. Applications include the monitoring of multiple molecular events, cell trafficking and targeting in tumorigenesis studies, cancer diagnosis, metastasis detection, drug discovery and development, gene therapy, and orthopedic research [3,6–8]. Molecular imaging is broadly based on three technologies: nuclear imaging [9,10], magnetic resonance imaging (MRI) [11,12], and optical imaging [13,14]. Numerous instrumentations have been developed based on the three technologies. For instance, nuclear imaging includes positron emission tomography (PET) [15–17] and single photon emission computed tomography (SPECT) [18], while optical imaging mainly involves fluorescence molecular tomography (FMT) [14,19] and bioluminescent imaging (BLI) [20–22]. The difference between FMT and BLI are discussed in [23]. Different technologies can also be used in a combined system [25].

BLT has received considerable attention in recent years because of its advantages regarding sensitivity and specificity. A major issue in BLT is the determination of the distribution of a bioluminescent source. With the

X. Cheng · R. Gong (✉)
Department of Mathematics, Zhejiang University, Hangzhou 310027, People's Republic of China
e-mail: gongrongfang319@yahoo.com.cn; grf_zju@163.com

X. Cheng
e-mail: xiaoliangcheng@zju.edu.cn

W. Han
Department of Mathematics, University of Iowa, Iowa City, IA 52242, USA
e-mail: whan@math.uiowa.edu

introduction of BLT, a bioluminescent-source distribution inside a living small animal can be localized and quantified in three dimensions. In the absence of BLT, bioluminescence imaging is primarily qualitative. With BLT, quantitative and localized analysis of a bioluminescent-source distribution becomes feasible in a living subject [24–28]. In BLT, an internal bioluminescent source is constructed from a measured bioluminescent signal on the external surface of a small animal. The problem of determining the photon density on the small animal surface from the bioluminescent-source distribution inside the animal requires accurate representation of photon transport in biological tissue. The bioluminescent-photon propagation in biological tissue can be well described by either a radiative-transfer equation (RTE) or a Monte Carlo model. However, at present, because transmission of the bioluminescent photons through the biological tissue is subject to both scattering and absorption, neither description is computationally feasible in most practical applications. In practical implementation, approximation of the diffusion equation of RTE is chosen if scattering is dominant over absorption in the process of propagation of light inside a small animal [29].

In Sect. 2, a mathematical statement of the BLT problem is given. In Sect. 3, a new formulation for BLT is introduced, based on the use of an adjoint equation. In Sect. 4, the discretization of the new formulation by the finite-element method is discussed. Several numerical examples are presented in Sect. 5 to demonstrate the feasibility of the proposed method. Concluding remarks are given in the last section.

2 Problem statement

Let $\Omega \subset \mathbb{R}^3$ with boundary Γ of class $C^{0,1}$ be the domain occupied by a biological medium. We denote by $u_0 = u_0(x, \theta, t)$ the light flux in direction $\theta \in S^2$ (S^2: the unit sphere) at $x \in \Omega$ and $t > 0$, and by $p_0 = p_0(x, \theta, t)$ the internal light source. Light transport in the biological tissue can be described by RTE [29,30],

$$\frac{1}{c}\frac{\partial u_0}{\partial t} + \theta \cdot \nabla_x u_0 + \mu u = \mu_s \int_{S^2} k(\theta \cdot \theta') u_0(x, \theta', t)\, \mathrm{d}\theta' + p_0 \quad \text{in } \Omega, \tag{1}$$

where c is the photon speed, $\mu = \mu_a + \mu_s$, and μ_a, μ_s are absorption and scattering coefficients. The scattering kernel function $k \geq 0$ is such that $\int_{S^2} k(\theta \cdot \theta')\, \mathrm{d}\theta' = 1$. The initial and boundary conditions for equation (1) are

$$u_0(x, \theta, 0) = 0, \quad x \in \Omega,\ \theta \in S^2$$

and

$$u_0(x, \theta, t) = g^-(x, \theta, t), \quad t > 0,\ x \in \Gamma,\ \theta \in S^2 \text{ such that } \nu(x) \cdot \theta \leq 0,$$

respectively, where ∂_ν is the outward-normal differentiation operator on the boundary Γ. To reconstruct the internal light source p_0, we consider measurements of the outgoing radiation on the boundary Γ:

$$g(x, t) = \int_{S^2} \nu(x) \cdot \theta u_0(x, \theta, t)\, \mathrm{d}\theta, \quad t > 0,\ x \in \Gamma.$$

Because the RTE is highly dimensional, it presents a serious challenge for accurate numerical simulations, given the current level of development of computer software and hardware. However, because the mean-free path of the photon is between 500 nm and 1,000 nm in biological tissues, which is very small compared to a typical object in this context, scattering dominates transport [29]. Since the internal bioluminescence distribution induced by reporter genes is relatively stable, we neglect the time dependence. The diffusion approximation of the RTE (1) is (see [31,32] for detail)

$$-\operatorname{div}(D\nabla u) + \mu_a u = p \quad \text{in } \Omega. \tag{2}$$

Here $u = u(x)$ and $p = p(x)$, defined as

$$u(x) = \frac{1}{4\pi}\int_{S^2} u_0(x, \theta)\, \mathrm{d}\theta, \quad p(x) = \frac{1}{4\pi}\int_{S^2} p_0(x, \theta)\, \mathrm{d}\theta,$$

are the average light flux and average light-source distribution in any direction respectively, $D = [3(\mu_a + \mu_s^{'})]^{-1}$, $\mu_s^{'} = (1 - \overline{k})\mu_s$ is the reduced scattering coefficient with

$$\overline{k} = \frac{1}{4\pi} \int_{S^2} \theta \cdot \theta' k(\theta \cdot \theta') \, \mathrm{d}\theta'.$$

Accordingly, the boundary condition reduces to

$$u + 2D\partial_\nu u = g^- \equiv g_2 \quad \text{on } \Gamma, \tag{3}$$

while the boundary measurement reduces to

$$g = -D\partial_\nu u \quad \text{on } \Gamma. \tag{4}$$

From (3) and (4), we obtain a third boundary condition for Eq. 2,

$$u = g^- + 2g \equiv g_1 \quad \text{on } \Gamma. \tag{5}$$

Note that only two of the three boundary conditions (3), (4) and (5) are independent. As pointed out in [26], to determine the source function p, we may associate one of the above three boundary conditions (3), (4) and (5) with the differential equation (2) to form a boundary-value problem, while choosing one of the remaining boundary conditions to form an inverse problem for p. In [26], the inverse problem was discussed for the boundary-value problem (2) and (3) with the measurement matching for (5):

Problem 1 Given $D > 0$, $\mu_a \geq 0$, g_1 and g_2, suitably smooth, find a source function p such that the solution of the boundary-value problem,

$$\begin{cases} -\mathrm{div}(D\nabla u) + \mu_a u = p\chi_{\Omega_0} & \text{in } \Omega \\ u + 2D\partial_\nu u = g_2 & \text{on } \Gamma, \end{cases} \tag{6}$$

satisfies

$$u = g_1 \quad \text{on } \Gamma. \tag{7}$$

Here Ω_0 is a measurable subset of Ω, known as the permissible region, χ_{Ω_0} is the characteristic function of Ω_0, i.e., its value is 1 in Ω_0 and is 0 outside Ω_0. Even with this simplification, it still remains to develop efficient ways of simulating diffusion-based BLT [26–28,33–36].

Next, we discuss, BLT problem based on Problem 1. The purpose of this paper is to introduce a new formulation as the basis of a potentially more effective numerical method to solve the BLT problem. Different from conventional ways, which often involve minimizing a cost functional subject to a system of differential equations, we convert the determination of a source function p to the problem of solving a system of equations. In this way, the BLT problem is solved through linear systems of elliptic partial differential equations by passing optimization. We will see that our new method provides good numerical results.

In what follows, we let Ω be a domain in $\mathbb{R}^d$ ($d = 3$ for applications) with boundary Γ. Moreover, for our future needs, we introduce a few symbols. For $G = \Omega$, Ω_0 or Γ, and $s \geq 0$, we denote by $H^s(G)$ the standard Sobolev space associated with inner product $(\cdot, \cdot)_{s,G}$ and norm $\|\cdot\|_{s,G}$, $H^0(G) = L^2(G)$. Denote $V = H^1(\Omega)$, $V_0 = H_0^1(\Omega)$ and $Q = L^2(\Omega_0)$.

For any $q \in Q$, we denote by $u = u(q) \in V$ the solution of the problem

$$\int_\Omega (D\nabla u \cdot \nabla v + \mu_a u v) \, \mathrm{d}x + \frac{1}{2} \int_\Gamma u v \, \mathrm{d}s = \int_{\Omega_0} q v \, \mathrm{d}x + \frac{1}{2} \int_\Gamma g_2 v \, \mathrm{d}s \quad \forall v \in V. \tag{8}$$

This is a weak formulation of the boundary-value problem defined by (6) with p replaced by q. Suppose that the admissible source function p belongs to a closed convex subset Q_{ad} of the space Q.

Problem 1 is usually studied via a least-squares optimization approach.

Problem 2 Find $p \in Q_{\text{ad}}$ such that

$$J(p) = \inf_{q \in Q_{\text{ad}}} J(q),$$

where

$$J(q) = \frac{1}{2} \|u(q) - g_1\|_{0,\Gamma}^2.$$

As noted in [26], Problems 1 and 2 are ill-posed. In general, there are infinitely many solutions. When the form of the source function is pre-specified, there is no solution if the data are inconsistent. Moreover, the source function does not depend continuously on the data. To circumvent these difficulties, a Tikhonov-type regularization version of the problem is introduced and numerically solved. Define a functional

$$J_\varepsilon(q) = \frac{1}{2} \|u(q) - g_1\|_{0,\Gamma}^2 + \frac{\varepsilon}{2} \|q\|_{0,\Omega_0}^2, \quad \varepsilon \geq 0.$$

Then for BLT reconstruction, we study the following constrained optimization problem.

Problem 3 Find $p_\varepsilon \in Q_{\text{ad}}$ such that

$$J_\varepsilon(p_\varepsilon) = \inf_{q \in Q_{\text{ad}}} J_\varepsilon(q).$$

By Theorems 3.2 and 3.3 in [26], this reformulation is well-posed for $\varepsilon > 0$. Moreover, it is shown there that the reformulated problem with $\varepsilon > 0$ permits stable and convergent numerical solutions.

3 A new formulation for BLT

Our main objective in this section is to introduce a new formulation for studying the BLT problem. Let $\Omega \subset \mathbb{R}^d$ be an open and bounded convex set with boundary Γ. It is shown in [37, Sect. 1.2] that the boundary of an open, bounded and convex set is Lipschitz continuous; consequently, the unit outward normal vector exists on Γ. Assume that the coefficients D, μ_a and measurements g_1, g_2 belongs to space $L^\infty(\Omega)$ such that $D \geq D_0$ in Ω for some constant $D_0 > 0$, $\mu_a \geq 0$ a.e. in Ω, and $\mu_a > 0$ a.e. in a subset of Ω with positive measure.

For the derivation of our new formulation for BLT, let $u = u(q)$ be the solution of problem

$$\begin{cases} -\text{div}(D\nabla u) + \mu_a u = q\chi_{\Omega_0} & \text{in } \Omega \\ u + 2D\partial_\nu u = g_2 & \text{on } \Gamma. \end{cases} \tag{9}$$

Denote by $u^* = u(p_\varepsilon)$ and $\widetilde{u}$ the solutions of the problems

$$\begin{cases} -\text{div}(D\nabla u^*) + \mu_a u^* = p_\varepsilon \chi_{\Omega_0} & \text{in } \Omega \\ u^* + 2D\partial_\nu u^* = g_2 & \text{on } \Gamma \end{cases} \tag{10}$$

and

$$\begin{cases} -\text{div}(D\nabla \widetilde{u}) + \mu_a \widetilde{u} = q\chi_{\Omega_0} & \text{in } \Omega \\ \widetilde{u} + 2D\partial_\nu \widetilde{u} = 0 & \text{on } \Gamma, \end{cases} \tag{11}$$

respectively. Together with problem (9), we have, for any $q \in Q_{\text{ad}}$, $u(p_\varepsilon + tq) = u^* + t\,\widetilde{u}$. Then, for any $t \in \mathbb{R}$ and $q \in Q_{\text{ad}}$,

$$\begin{aligned} J_\varepsilon(p_\varepsilon + tq) - J_\varepsilon(p_\varepsilon) = {} & \frac{1}{2}\int_\Gamma [u(p_\varepsilon + tq) - g_1]^2 \, \mathrm{d}s + \frac{\varepsilon}{2}\int_{\Omega_0} (p_\varepsilon + tq)^2 \, \mathrm{d}x \\ & - \frac{1}{2}\int_\Gamma (u^* - g_1)^2 \, \mathrm{d}s - \frac{\varepsilon}{2}\int_{\Omega_0} p_\varepsilon^2 \, \mathrm{d}x = t\left[\int_\Gamma (u^* - g_1)\,\widetilde{u}\,\mathrm{d}s + \varepsilon \int_{\Omega_0} p_\varepsilon\, q \mathrm{d}x\right] \\ & + \frac{t^2}{2}\left(\int_\Gamma \widetilde{u}^2 \, \mathrm{d}s + \varepsilon \int_{\Omega_0} q^2 \, \mathrm{d}x\right) \end{aligned}$$

and the Gateaux derivative of J_ε at p_ε in the direction of $q \in Q_{\text{ad}}$ is

$$J'_\varepsilon(p_\varepsilon)\, q = \lim_{t\to 0} \frac{J_\varepsilon(p_\varepsilon + tq) - J_\varepsilon(p_\varepsilon)}{t} = \int_\Gamma (u^* - g_1)\, \widetilde{u}\, \mathrm{d}s + \varepsilon \int_{\Omega_0} p_\varepsilon\, q\, \mathrm{d}x. \tag{12}$$

Let w be the solution of the adjoint problem

$$\begin{cases} -\mathrm{div}(D\nabla w) + \mu_a\, w = 0 & \text{in } \Omega \\ w + 2D\partial_\nu w = u^* - g_1 & \text{on } \Gamma. \end{cases} \tag{13}$$

We multiply (13) by $\widetilde{u}$, integrate over Ω and integrate by parts to get

$$\int_\Omega (D\nabla w \cdot \nabla \widetilde{u} + \mu_a\, w\, \widetilde{u})\, \mathrm{d}x + \frac{1}{2}\int_\Gamma w\, \widetilde{u}\, \mathrm{d}s = \frac{1}{2}\int_\Gamma (u^* - g_1)\, \widetilde{u}\, \mathrm{d}s. \tag{14}$$

Similarly, from (11), we obtain

$$\int_\Omega (D\nabla w \cdot \nabla \widetilde{u} + \mu_a\, w\, \widetilde{u})\, \mathrm{d}x + \frac{1}{2}\int_\Gamma \widetilde{u}\, w\, \mathrm{d}s = \int_{\Omega_0} q\, w\, \mathrm{d}x. \tag{15}$$

Combining (14), (15) and (12), we obtain

$$J'_\varepsilon(p_\varepsilon)\, q = \int_{\Omega_0} (2w + \varepsilon p_\varepsilon)\, q \mathrm{d}x. \tag{16}$$

Because Q_{ad} is a convex and closed subset of space Q, the following first-order necessary and sufficient condition [38,39] of the solution $p_\varepsilon \in Q_{\text{ad}}$ of Problem 3 holds:

$$J'_\varepsilon(p_\varepsilon)\,(q - p_\varepsilon) \geq 0 \quad \forall q \in Q_{\text{ad}}$$

or

$$\int_{\Omega_0} (2w + \varepsilon p_\varepsilon)\,(q - p_\varepsilon)\, \mathrm{d}x \geq 0 \quad \forall q \in Q_{\text{ad}}.$$

Therefore, p_ε is the projection of $-2w/\varepsilon$ on Q_{ad} with respect to the $L^2(\Omega_0)$ inner product ([38, Sect. 5.3]). If Q_{ad} consists of the non-negatively valued $L^2(\Omega_0)$ functions, we have

$$p_\varepsilon = \max\left\{-\frac{2}{\varepsilon}w, 0\right\} \quad \text{in } \Omega_0.$$

If $Q_{\text{ad}} = Q$, then

$$p_\varepsilon = -\frac{2}{\varepsilon}w \quad \text{in } \Omega_0. \tag{17}$$

This holds when $-2w/\varepsilon \in Q_{\text{ad}}$. Consequently, we consider the following equations and boundary conditions:

$$\begin{cases} -\mathrm{div}(D\nabla u^*) + \mu_a u^* + \frac{2}{\varepsilon} w \chi_{\Omega_0} = 0 & \text{in } \Omega \\ -\mathrm{div}(D\nabla w) + \mu_a w = 0 & \text{in } \Omega \\ p_\varepsilon = -\frac{2}{\varepsilon} w & \text{in } \Omega_0 \\ u^* + 2D\partial_\nu u^* = g_2 & \text{on } \Gamma \\ w + 2D\partial_\nu w = u^* - g_1 & \text{on } \Gamma. \end{cases} \tag{18}$$

A new formulation for studying the BLT problem follows.

Problem 4 Find $(u^*, w) \in V \times V$ such that

$$\begin{cases} a(u^*, v) + b_1(w, v) = f_1(v) & \forall\, v \in V, \\ b_2(u^*, v) + a(w, v) = f_2(v) & \forall\, v \in V, \\ p_\varepsilon = -\frac{2}{\varepsilon} w & \text{in } \Omega_0, \end{cases} \tag{19}$$

where

$$a(u, v) = \int_\Omega (D\nabla u \cdot \nabla v + \mu_a u\, v)\, \mathrm{d}x + \frac{1}{2}\int_\Gamma u\, v\, \mathrm{d}s, \quad b_1(u, v) = \int_{\Omega_0} \frac{2}{\varepsilon} u\, v\, \mathrm{d}x,$$

$$b_2(u, v) = -\frac{1}{2}\int_\Gamma u\, v\, \mathrm{d}s, \quad f_1(v) = \frac{1}{2}\int_\Gamma g_2\, v\, \mathrm{d}s, \quad f_2(v) = -\frac{1}{2}\int_\Gamma g_1\, v\, \mathrm{d}s.$$

Next, we focus on the numerical performance of the new formulation.

4 Finite-element approximation

In this section, we consider the problem of approximating the solution of Problem 4 with FEMs. For simplicity, we assume that both $\Omega \subset \mathbb{R}^d$ and $\Omega_0 \subset \Omega$ are polyhedral convex set. We note that Ω and Ω_0 can be any bounded open convex domains. Let $\{\mathcal{T}_h\}_h$ and $\{\mathcal{T}_{0,H}\}_H$ be regular families of finite-element partitions of $\overline{\Omega}$ and $\overline{\Omega_0}$, respectively. For any triangulation $\mathcal{T}_h = \{K\}$, $\mathcal{T}_{0,H} = \{T\}$, define the finite-element spaces

$$V^h = \{v \in C(\Omega) \mid v\,|_K \in \mathcal{P}_K^k \text{ or } \mathcal{Q}_K^k \quad \forall K \in \mathcal{T}_h\},$$

$$Q^H = \{q \in Q \mid q|_T \in \mathcal{P}_T^t \text{ or } \mathcal{Q}_T^t \quad \forall T \in \mathcal{T}_{0,H}\},$$

where $\mathcal{P}_G^s$ and $\mathcal{Q}_G^s$ denote spaces of polynomials over the set G of total degree and individual degree less than or equal to s, respectively. Denote by Π^H the orthogonal projection operator from space Q onto space Q^H:

$$(\Pi^H p, q^H)_{0,\Omega_0} = (p, q^H)_{0,\Omega_0} \quad \forall p \in Q,\ q^H \in Q^H. \tag{20}$$

Then we have an approximation to continuous Problem 4 as follows.

Problem 5 Find $(u_h^*, w_h) \in V^h \times V^h$ such that

$$\begin{cases} a(u_h^*, v_h) + b_1(w_h, v_h) = f_1(v_h) & \forall\, v \in V^h, \\ b_2(u_h^*, v_h) + a(w_h, v_h) = f_2(v_h) & \forall\, v \in V^h, \\ p_{\varepsilon,h}^H = -\frac{2}{\varepsilon} w_h^H = -\frac{2}{\varepsilon}\Pi^H w_h & \text{in } \Omega_0. \end{cases} \tag{21}$$

Let $\varphi_i(x) \in V^h$, $i = 1, 2, \ldots, n$ be the node basis functions of finite-element space V^h associated with grid nodes x_i, where n is the number of the nodes of triangulation $\mathcal{T}_h$. Then the solution $u_h^* \in V^h$ can be written as $u_h^* = \sum_{i=1}^n u_i^* \varphi_i$, where u_i^* denotes the value of function u^* at grid node x_i, i.e., $u_i^* = u^*(x_i)$. Similarly, w_h can be expanded by $w_h = \sum_{i=1}^n w_i \varphi_i$ with $w_i = w(x_i)$. Moreover, let $\phi_s(x) \in Q^H$, $s = 1, 2, \ldots, N$ (N is the number of the nodes of triangulation $\mathcal{T}_{0,H}$), be the node basis functions of finite-element space Q^H associated with grid nodes x_s, and denote $\varphi_{0,l}$, $l = 1, 2, \ldots, N_0$, for those basis functions associated with nodes $x_{0,l}$ contained in $\overline{\Omega_0}$.

Then Problem 5 is equivalent to the following.

Problem 6 Solve linear system

$$KY = F, \tag{22}$$

and compute the approximation light-source function p by

$$p_{\varepsilon,h}^H = -\frac{2}{\varepsilon}\sum_{s=1}^{N}\left(\sum_{l=1}^{N_0} w_l \varphi_{0,l}(x_s)\right)\phi_s \quad \text{in } \Omega_0, \tag{23}$$

where

$$K \triangleq \begin{pmatrix} A & B_1 \\ B_2 & A \end{pmatrix}, \quad Y \triangleq (U^t, W^t)^t, \quad F \triangleq (F_1^t, F_2^t)^t,$$

$$U = (u_1^*, u_2^*, \ldots, u_n^*)^t, \quad W = (w_1, w_2, \ldots, w_n)^t, \quad F_k = (f_{k1}, f_{k2}, \ldots, f_{kn})^t,$$

$$f_{kj} = f_k(\varphi_j), \quad A = (a^{ji}), \quad a^{ji} = a(\varphi_i, \varphi_j), \quad B_1 = (b_1^{ji}), \quad b_1^{ji} = b_1(\varphi_i, \varphi_j),$$

$$B_2 = (b_2^{ji}), \quad b_2^{ji} = b_2(\varphi_i, \varphi_j), \quad i, j = 1, 2, \ldots, n,\ k = 1, 2,$$

and $(\cdot)^t$ is the transposition of $(\cdot)$.

We note that if $\mathcal{T}_h = \{K\}$ and $\mathcal{T}_{0,H} = \{T\}$ are consistent, then $H = h$, $N = N_0$ and (23) reduces to

$$p_{\varepsilon,h}^h = -\frac{2}{\varepsilon}\sum_{s=1}^{N} w_s \phi_s \quad \text{in } \Omega_0. \tag{24}$$

5 Numerical examples

In this section, we present numerical results for two model problems. Our goal is to demonstrate the feasibility of our new formulation for the BLT problem. Let Ω be the problem domain and Ω_0 be the permissible region. Assume an absorption coefficient $\mu_a \equiv 0.02$ and a reduced scattering coefficient $\mu_s' \equiv 1.00$ in Ω. We use uniform square partitions of the regions $\overline{\Omega}$ and $\overline{\Omega_0}$ with mesh parameters $h = H$, where h and H are the maximal diameters of the elements in the partitions $\mathcal{T}_h$ and $\mathcal{T}_{0,H}$, respectively. For finite-element spaces V^h and Q^h, we use continuous piecewise bilinear functions and piecewise constant functions corresponding to the partitions $\mathcal{T}_h$ and $\mathcal{T}_{0,h}$. From the boundary value of a finite-element solution of BVP (2)–(3) for a small enough meshsize we compute the function g_1; in our experiment, we choose $1/512$ for this small meshsize. In the following, we compute the approximate source function $p^h_{\varepsilon,h}$ for different grid parameter h and different regularization parameter ε.

5.1 Model 1

In this model, we have $\Omega = (0, 1) \times (0, 1)$, $\Omega_0 = (0.5, 0.75) \times (0.5, 0.75)$, $p \equiv 1$ pW for the true light source in Ω_0, and set $g_2 \equiv 0$ on the boundary $\Gamma = \partial\Omega$. Denote the error $E = p^h_{\varepsilon,h} - p$.

We first demonstrate the performance of the solution $p^h_{\varepsilon,h}$ of BLT obtained from our new formulation when the data g_1 and g_2 are noise-free. For different meshsize and regularization parameter, we reconstruct light-source functions $p^h_{\varepsilon,h}$ and plot one of them in Fig. 1 for $h = 1/64$ and $\varepsilon = 10^{-5}$. Tables 1–2 show the dependence of the error in the approximate light-source function $p^h_{\varepsilon,h}$ on the meshsize and regularization parameter, respectively. Note that $\|\cdot\|_\infty$ and $\|\cdot\|_0$ are the L^∞ and L^2 norms, respectively. The accuracy of discrete solution improves as h or ε gets smaller. Further features of the discrete solution can be seen from Figs. 2–3. Figure 2 shows the error of

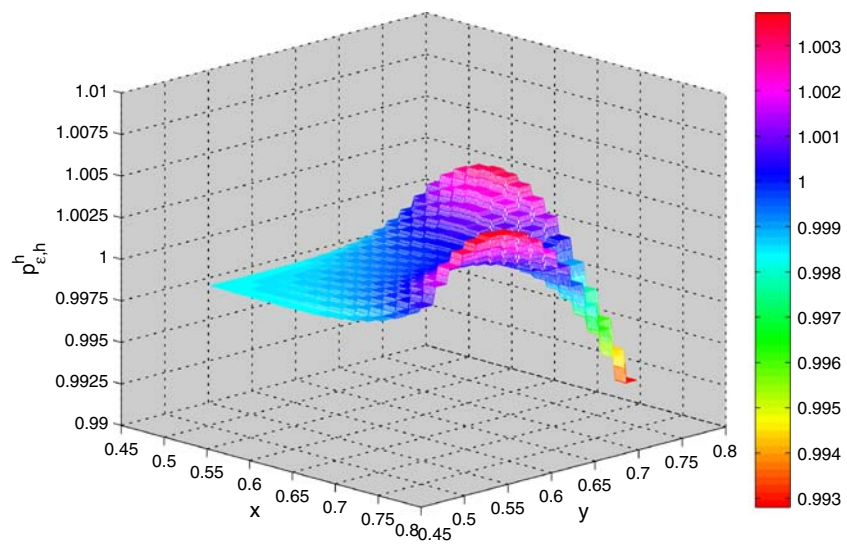

Fig. 1 Model 1: Reconstructed light-source function $p^h_{\varepsilon,h}$ for meshsize $h = 1/64$ and regularization parameter $\varepsilon = 10^{-5}$

Table 1 Model 1: Error in approximate light-source function $p^h_{\varepsilon,h}$ for regularization parameter $\varepsilon = 10^{-5}$

h	1/4	1/8	1/16	1/32	1/64	1/128
$\|E\|_\infty$	4.1211	3.4971×10^{-1}	5.9186×10^{-2}	2.1386×10^{-2}	7.1987×10^{-3}	2.8881×10^{-3}
$\|E\|_0$	1.0303	4.7054×10^{-2}	5.2836×10^{-3}	1.2056×10^{-3}	3.8184×10^{-4}	2.0781×10^{-4}

Table 2 Model 1: Error in approximate light-source function $p^h_{\varepsilon,h}$ for meshsize $h = 1/64$

ε	10^{-1}	10^{-2}	10^{-3}	10^{-4}	10^{-5}
$\|E\|_\infty$	6.2449×10^{-1}	1.7197×10^{-1}	4.5229×10^{-2}	1.0708×10^{-2}	7.1987×10^{-3}
$\|E\|_0$	1.5149×10^{-1}	3.3547×10^{-2}	4.9663×10^{-3}	9.1736×10^{-4}	3.8184×10^{-4}

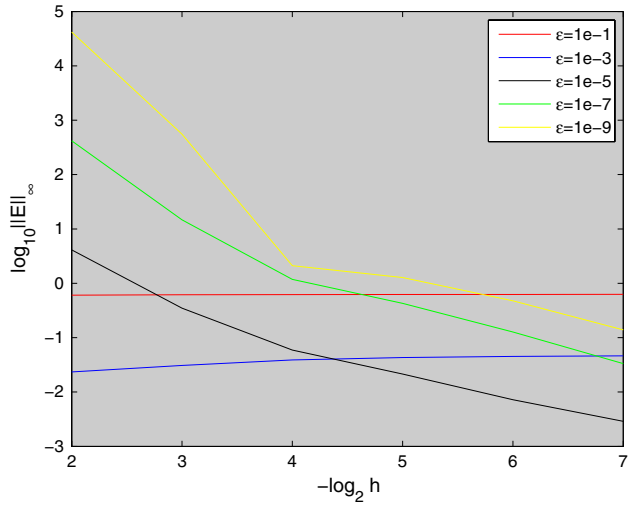

Fig. 2 Model 1: Error in approximate light-source function $p^h_{\varepsilon,h}$ against meshsize h in scale $-\log_2$ and $\log_{10}$, respectively, for different values of regularization parameter ε

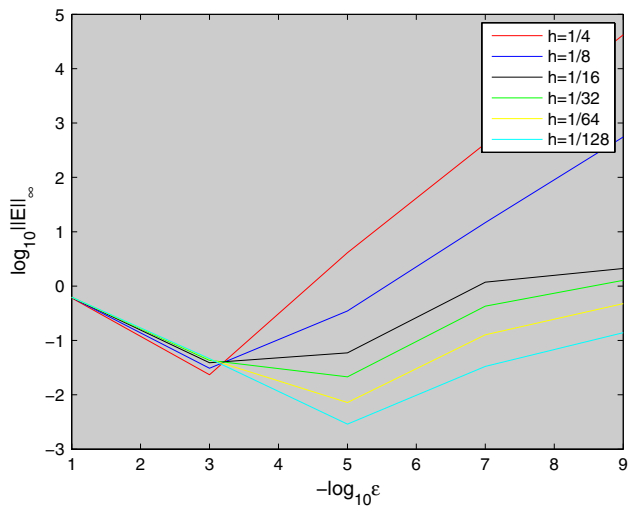

Fig. 3 Model 1: Error in approximate light-source function $p^h_{\varepsilon,h}$ against regularization parameter ε in scale $-\log_{10}$ and $\log_{10}$, respectively, for different values of meshsize h

the approximate solution in the norm L^∞ versus (vs.) the meshsize. The red, blue, black, green and yellow curves correspond to parameter $\varepsilon = 10^{-1}, 10^{-3}, 10^{-5}, 10^{-7}$, and 10^{-9}, respectively. It appears that $\varepsilon = 10^{-5}$ is a best choice (the black curve in Fig. 2). Figure 3 plots the error against the regularization parameter. These figures suggest that values of h and ε should match in order to achieve optimal numerical performance.

To examine the stability of our modality, we introduce random noise on the observation data g_1 with three noise level, $\delta = 1\%$, 10%, and 20%. For each noise level δ, we compute the discrete solution $p^h_{\varepsilon,h}$ ten times and use the average error of the corresponding solutions as the error of the approximate solution associated with δ. Figure 4 plots the L^∞ norm of the error of the approximate solution agianst the meshsize h for four noise levels, 0, 1%, 10%, and 20%. Higher noise level leads to higher solution error. The same conclusion can be drawn from Fig. 5 for

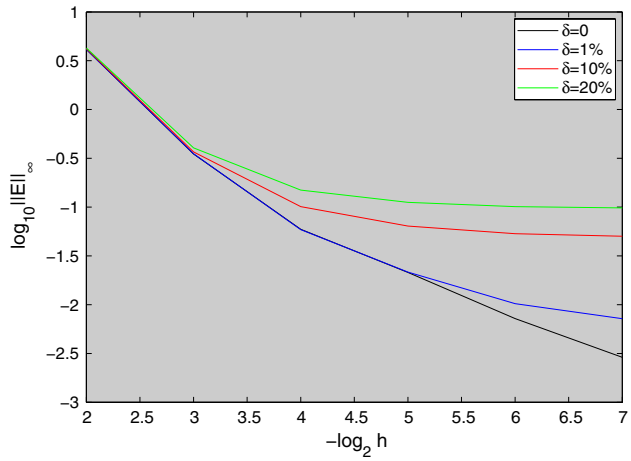

Fig. 4 Model 1: Error in approximate light-source function $p^h_{\varepsilon,h}$ against meshsize h in scale $-\log_2$ and $\log_{10}$, respectively, for different values of noise level δ when regularization parameter $\varepsilon = 10^{-5}$

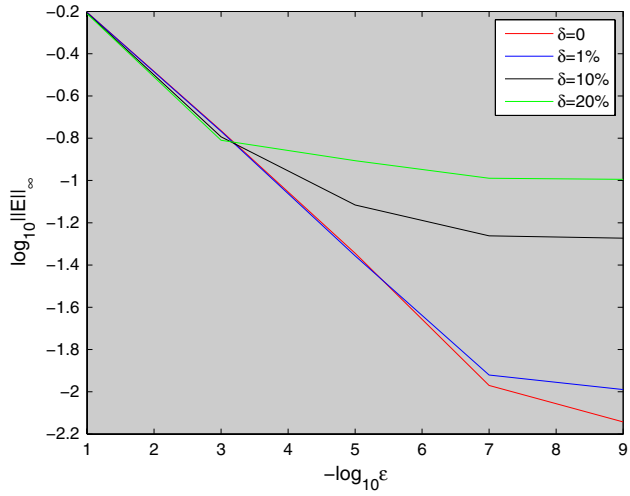

Fig. 5 Model 1: Error in approximate light-source function $p^h_{\varepsilon,h}$ against regularization parameter ε in scale $-\log_{10}$ and $\log_{10}$, respectively, for different values of noise level δ when meshsize $h = 1/64$

the error of the approximate solution in L^∞ norm against the regularization parameter ε. These numerical results clearly demonstrate that the numerical solution is stable with respect to the perturbation in the measurement data.

5.2 Model 2

In the second model, we assume that the permissible region Ω_0 of light-source function is the union of k disjoint subdomains Ω_{0i}, $i = 1, 2, \ldots, k$. In our simulation, we take $k = 4$, $\Omega_{01} = (0.25, 0.375) \times (0.25, 0.375)$, $\Omega_{02} = (0.625, 0.75) \times (0.25, 0.375)$, $\Omega_{03} = (0.25, 0.375) \times (0.625, 0.75)$ and $\Omega_{04} = (0.625, 0.75) \times (0.625, 0.75)$. The true light-source function is piecewise constant: $p(x) = p_i$ in Ω_{0i}, $i = 1, 2, 3, 4$; we take $p_1 = 1.0$, $p_2 = 1.3$, $p_3 = 1.0$ and $p_4 = 1.3$. Again we let $H = h$ and $g_2 \equiv 0$ on the boundary $\Gamma = \partial\Omega$.

Similar to Model 1, we consider boundary measurement g_1 with or without noise, obtaining similar results. A reconstructed light source $p^h_{\varepsilon,h}$ is shown in Fig. 6. Tables 3 and 4 show the dependence of the error in both L^∞ and L^2–norms in the approximate light-source function on the meshsize h and regularization parameter ε. Numerical results corresponding to noise-free data and noise data are reported in Figs. 7–8 and in Figs. 9–10, respectively.

We conclude this section by emphasizing that the numerical values of $-\frac{2}{\varepsilon} w^H_h$ in Ω_0 are always non-negative in our numerical experiments, and this justifies the use of (17) in these examples.

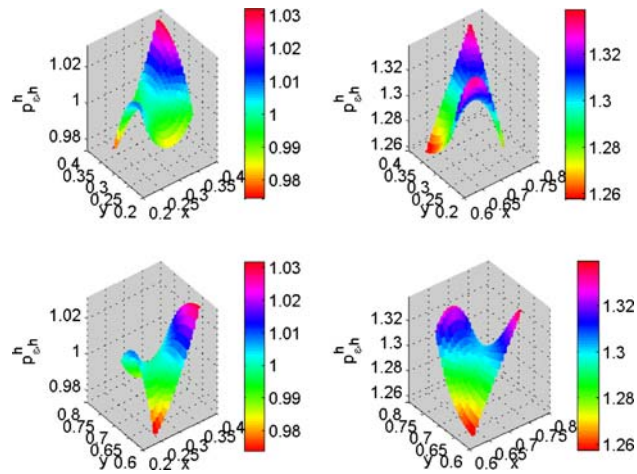

Fig. 6 Model 2: Reconstructed light-source function $p^h_{\varepsilon,h}$ for meshsize $h = 1/128$ and regularization parameter $\varepsilon = 10^{-7}$

Table 3 Model 2: Error in approximate light-source function $p^h_{\varepsilon,h}$ for regularization parameter $\varepsilon = 10^{-10}$

h	1/8	1/16	1/32	1/64	1/128
$\|E\|_\infty$	1.1511×10^{1}	1.9453	4.9522×10^{-1}	2.1376×10^{-1}	1.4795×10^{-1}
$\|E\|_0$	1.4389	1.4762×10^{-1}	2.8379×10^{-2}	9.1141×10^{-3}	6.9120×10^{-3}

Table 4 Model 2: Error in approximate light-source function $p^h_{\varepsilon,h}$ for meshsize $h = 1/128$

ε	10^{-1}	10^{-3}	10^{-5}	10^{-7}	10^{-9}
$\|E\|_\infty$	2.8833	2.6776×10^{-1}	2.0564×10^{-1}	1.4795×10^{-1}	6.7984×10^{-1}
$\|E\|_0$	3.5897×10^{-1}	1.9108×10^{-2}	1.1957×10^{-2}	6.9120×10^{-3}	1.8558×10^{-2}

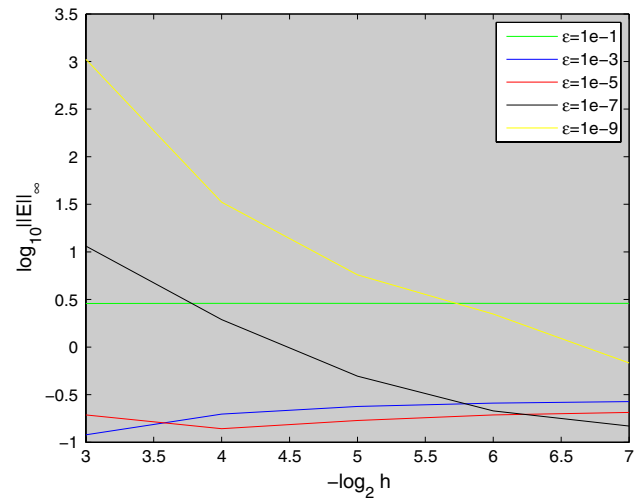

Fig. 7 Model 2: Error in the approximate light-source function $p^h_{\varepsilon,h}$ against meshsize h in scale $-\log_2$ and $\log_{10}$, respectively, for different values of regularization parameter ε

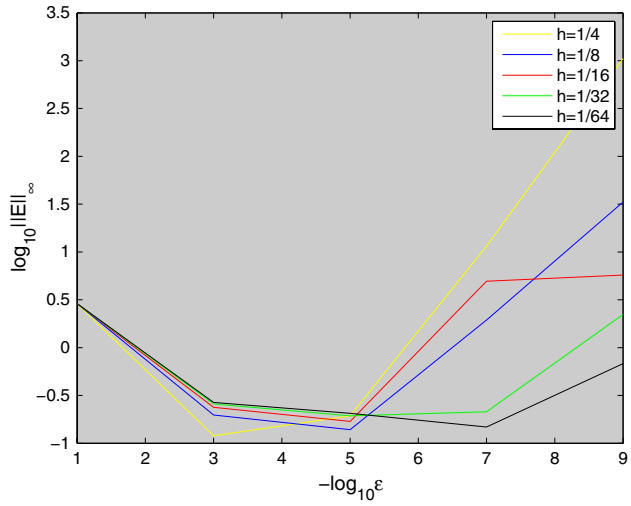

Fig. 8 Model 2: Error in the approximate light-source function $p^h_{\varepsilon,h}$ against regularization parameter ε in scale $-\log_{10}$ and $\log_{10}$, respectively, for different values of meshsize h

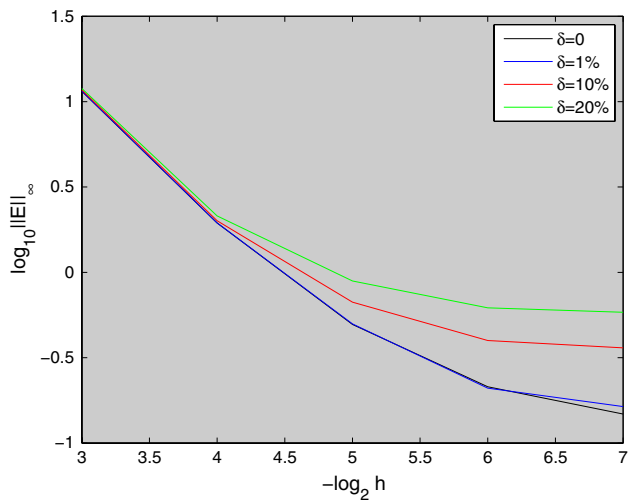

Fig. 9 Model 2: Error in the approximate light-source function $p^h_{\varepsilon,h}$ against meshsize h in scale $-\log_2$ and $\log_{10}$, respectively, for different values of noise level δ and regularization parameter $\varepsilon = 10^{-7}$

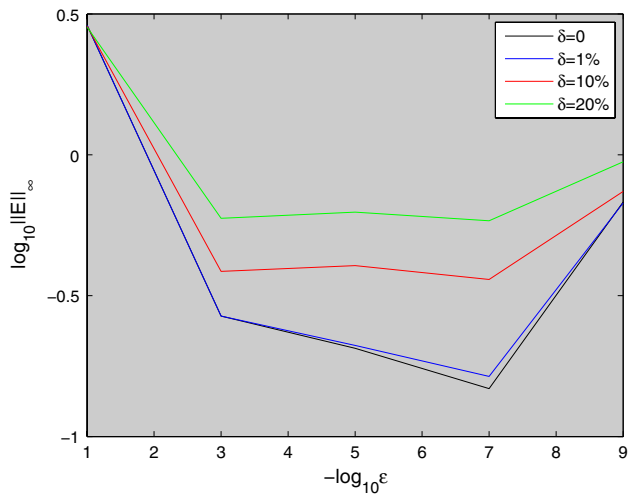

Fig. 10 Model 2: Error in approximate light-source function $p^h_{\varepsilon,h}$ vs. regularization parameter ε in scale $-\log_{10}$ and $\log_{10}$, respectively, for different values of noise level δ when meshsize $h = 1/128$

6 Conclusions

Bioluminescence tomography (BLT) is a promising new method, attracting increasing attention in the community of biomedical imaging. One major challenge is the development of efficient and effective numerical methods for solving the BLT problem. The aim of this paper is to explore an efficient method for obtaining a good approximation to the light source of the BLT problem. Because of the ill-posedness of the BLT, we adopt Tikhonov regularization. The conventional methods for the BLT problem are to treat it as a PDE constrained optimization problem (Problem 3). Consequently, numerical simulations are usually handled by an expensive iterative procedure where, at each iteration step, one needs to solve the BVP (8). In contrast, with our method we only need to solve the boundary-value problem (19) once. In this paper, FEMs have been applied to discretize PDEs for obtaining a approximate light-source function. Numerical experiments indicate that the method performs well.

Problem 4 and Problem 3 are identical only if p_ε from Problem 4 is non-negative, for the relevant BLT application. While currently there are no theoretical results that would guarantee the non-negativity of p_ε for Problem 4, numerical results on numerous simulations performed provide non-negative discrete light-source functions. If the non-negativity condition is violated for a numerical solution of Problem 4, the problem may be fixed through the use of a projection of the numerical solution of p_ε onto the admissible set Q_{ad}. If necessary, a few iterative solutions of the system (18) are performed where the $\frac{2}{\varepsilon}w$ term on the left-hand side of the first equation of (18) is replaced by the projected numerical values. This idea is currently under consideration.

The method proposed in this paper can be applied for source function reconstruction problems of more general PDEs if the admissible set Q_{ad} for the source function has a convexity structure such as non-negativity of function values.

Acknowledgements We thank the referees for their valuable comments that lead to an improvement on the presentation.

References

1. Cherry SR (2004) In vivo molecular and genomic imaging: new challenges for imaging physics. Phys Med Biol 49:13–48
2. Levin CS (2005) Primer on molecular imaging technology. Eur J Nucl Med Mol Imaging 32:325–345
3. Massoud TF, Gambhir SS (2003) Molecular imaging in living subjects: seeing fundamental biological processes in a new light. Genes Dev 17:545–580
4. Ray P, Wu AM, Gambhir SS (2003) Optical bioluminescence and bositron emission tomography imaging of a novel fusion reporter gene in tumor xenografts of living mice. Cancer Res 63:1160–1165
5. Troy T, Mcmullen DJ, Sambucetti L, Rice B (2004) Quantitative comparison of the sensitivity of detection of fluorescent and bioluminscent reporters in animal models. Mol Imaging 3:9–23
6. Bhaumik S, Gambhir SS (2002) Optical imaging of Renilla luciferase reporter gene expression in living mice. Proc Natl Acad Sci USA 99:377–382
7. Contag C, Bachmann MH (2002) Advances in bioluminescence imaging of gene expression. Annu Rev Biomed Eng 4:235–260
8. Kuckuk PM, Boskey AL (2006) Molecular imaging promotes progress in orthopedic research. Bone 39:965–977
9. Blasberg R (2002) Imaging gene expression and endogenous molecular processes: molecular imaging. J Cereb Blood Flow Metab 22:1157–1164
10. Gambhir SS (2002) Molecular imaging of cancer with positron emission tomography. Nat Rev Cancer 2:683–693
11. Genove G, DeMarco U, Xu H, Goins WF, Ahrens ET (2005) A new transgene reporter for in vivo magnetic resonance imaging. Nat Med 11:450–454
12. Weissleder R, Ntziachristos V (2003) Shedding light onto live molecular targets. Nat Med 9:123–128
13. Ntziachristos V, Ripoll J, Wang LV, Weissleder R (2005) Looking and listening to light: the evolution of whole-body photonic imaging. Nat Biotechnol 23:313–320
14. Ntziachristos V, Tung CH, Bremer C, Weissleder R (2002) Fluorescence molecular tomography resolves protease activity in vivo. Nat Med 8:757–760
15. Douraghy A, Prout DL, Silverman RW, Chatziioannou AF (2006) Evaluation of scintillator afterglow for use in a combined optical and PET imaging tomograph. Nucl Instrum Methods Phys Res A 569:557–562
16. Loo WTY, Tong JMK, Cheung MNB, Chow LWC (2006) A new predictive and prognostic marker (ATP bioluminescence and positron emission tomography) in vivo and in vitro for delivering adjuvant treatment plan to invasive breast tumor patients. Biomed Pharmacother 60:285–288

17. Serganova I, Moroz E, Moroz M, Pillarsetty N, Blasberg R (2006) Non-invasive molecular imaging and reporter genes. Cent Eur J Biol 1:88–123
18. Baumjohann D, Lutz MB (2006) Non-invasive imaging of dendritic cell migration in vivo. Immunobiol 211:587–597
19. Cong AX, Wang G (2006) Multispectral bioluminescence tomography: methodolgy and simulation. Int J Biomed Imaging 2006:Article ID 57614, 7 pp
20. Li SH, Driessen W, Sullivan S, Jiang HB (2006) Bioluminescence tomography based on phantoms with different concentrations of bioluminescent cancer cells. J Opt A: Pure Appl Opt 8:743–746
21. Chaudhari AJ, Darvas F, Bading JR, Moats RA, Conti PS, Smith DJ, Cherry SR, Leahy RM (2005) Hyperspectral and multispectral bioluminescence optical tomography for small animal imaging. Phys Med Biol 50:5421–5441
22. Doyle TC, Burns SM, Contag CH (2004) In vivo bioluminescence imaging for integrated studies of infection. Cell Microbiol 6:303–317
23. Hielscher AH (2005) Optical tomographic imaging of small animals. Curr Opin Biotechnol 16:79–88
24. Wang G, Hoffman EA et al (2003) Development of the first bioluminescent CT scanner. Radiol 229(P):566
25. Alexandrakis G, Rannou FR, Chatziioannou AF (2005) Tomographic bioluminescence imaging by use of a combined optical-PET (OPET) system: a computer simulation feasibility study. Phys Med Biol 50:4225–4241
26. Han W, Cong WX, Wang G (2006) Mathematical theory and numerical analysis of bioluminescence tomography. Inverse Probl 22:1659–1675
27. Han W, Cong WX, Wang G (2006) Mathematical study and numerical simulation of multispectral bioluminescence tomography. Int J Biomed Imaging 2006:Article ID 54390, 10 pp
28. Han W, Wang G (2007) Theoretial and numerical analysis on multispectral boluminescence tomography. IMA J Appl Math 72:67–85
29. Natterer F, Wabbeling F (2001) Mathematical methods in image reconstruction. SIAM, Philadephia
30. Arridge SR (1999) Optical tomography in medical imaging. Inverse Probl 15:R41–R93
31. Wang G, Li Y, Jiang M (2004) Uniqueness theorems in bioluminescence tomography. Med Phys 31:2289–2299
32. Han W, Wang G (2008) Bioluminescence tomography: biomedical background, mathematical theorey, and numerical approximation. J Comp Math 26:259–270
33. Cheng XL, Gong RF, Han W (2008) A new general mathematical framework for bioluminescence tomography. Comput Methods Appl Mech Eng 197:524–535
34. Cong WX, Durairaj K, Wang LV, Wang G (2006) A Born-type approximation method for bioluminescence tomography. Med Phys 33:679–686
35. Cong WX, Wang G, Kumar D et al (2005) A practical reconstruction method for bioluminescence tomography. Opt Exp 13:6756–6771
36. Lv YJ, Tian J, Cong WX, Wang G, Luo J, Yang W, Li H (2006) A multilevel adaptive finite element algorithm for bioluminescence tomography. Opt Exp 14:8211–8223
37. Grisvard P (1985) Elliptic problems in nonsmooth domains. Pitman, Boston
38. Atkinson K, Han W (2005) Theoretical numerical analysis: a functional analysis framework, 2nd edn. Springer-Verlag, New York
39. Lions J-L (1971) Optimal control of systems governed by partial differential equation. Springer, Berlin